Catal Lett (2009) 129:39–45
DOI 10.1007/s10562-009-9866-5

Carbon Nanotube Docking Stations: A New Concept in Catalysis

U. M. Graham · A. Dozier · R. A. Khatri · M. C. Bahome · L. L. Jewell · S. D. Mhlanga · N. J. Coville · B. H. Davis

Received: 19 December 2008 / Accepted: 12 January 2009 / Published online: 4 February 2009

Abstract The mobility of surface-bound metallic nanoparticles (NPs) on catalyst supports results in agglomeration leading to a subsequent decrease in effectiveness of the catalytic behavior of the metal NPs over time. We report here the synthesis and characterization of a carbon nanotube (CNT) catalyst support system enhanced with 'docking stations' along the exterior which limit the surface mobility of ultra small iron catalyst particles on CNT surfaces during Fisher–Tropsch synthesis.

Keywords Carbon nanotubes · Catalyst supports · Synfuels · Fisher–Tropsch synthesis · Surface reactivity

1 Introduction

Carbon nanotubes (CNTs) represent an appealing alternative to conventional catalyst supports based on the highly controllable surface properties [1, 2] that can be manipulated via functionalization of the outer CNT walls [3–5]. Alteration of CNT surfaces through mechanical deformation can have significant effects on the outer surface reactivity and chemical stability of CNTs since the macroscopic properties are controlled by the short and long-range ordering of atomic carbon [1, 6, 7]. Based on their large surface area [8] and many available adsorption sites [9, 10], CNTs in particular represent a distinctive class of metal catalyst supports that provide promising scenarios for enhanced chemical reactions including fuel synthesis [3, 11–15]. Production of synfuels via Fischer–Tropsch synthesis (FTS) process relies on nano-sized transition metal catalysts [16], predominantly iron or cobalt which have been previously supported on CNT outer walls [17, 18].

The Fischer–Tropsch synthesis (FTS) process takes syngas, a mixture of carbon monoxide (CO) and hydrogen (H_2), and converts it into hydrocarbon fuels over transition metal catalysts [19, 20]. Fuel synthesis via FTS is becoming increasingly important based on projected oil shortages, volatile crude oil prices, stringent environmental regulations and the fact that FTS can utilize syngas produced from several sources including biomass which helps control CO_2 emissions [21–23]. Iron and cobalt catalysts have been used industrially for FTS either unsupported or supported [24] with supports including CNT surfaces [11, 12, 17, 18, 25, 26]. Catalyst sintering, a process wherein the active metal nanoparticles agglomerate on support surface and lose effective surface area is a common mechanism of deactivation [27, 28]. In contrast, confinement of metal NPs inside the CNT main channel has been demonstrated recently to significantly enhance catalytic activity and stability over time during ethanol production [29] and Fischer-Tropsch synthesis [26] despite restricted

U. M. Graham · R. A. Khatri · B. H. Davis (✉)
Center for Applied Energy Research, University of Kentucky, 2540 Research Park Dr., Lexington, KY 40511, USA
e-mail: davis@caer.uky.edu

A. Dozier
Electron Microscopy Center, University of Kentucky, ASTeCC Bldg., Lexington, KY 40506, USA

M. C. Bahome · L. L. Jewell
School of Chemical and Metallurgical Engineering, University of Witwatersrand, 1 Jan Smuts Ave, Wits 2050, Johannesburg, South Africa

M. C. Bahome · S. D. Mhlanga · N. J. Coville
DST/NRF Center of Excellence in Strong Materials and Molecular Sciences Institute, School of Chemistry, University of Witwatersrand, 1 Jan Smuts Ave, Wits 2050, Johannesburg, South Africa

accessibility factors of the nanotube's main channel. A main reason for this enhanced catalytic activity and stability is said to be the structural confinement and, hence, drastically restricted migration ability of the catalyst particles which prevents agglomeration.

Three dimensional surface structures such as nanoscale ridges and valleys or wells on supports may offer new ways of protecting the ultra small catalyst against sintering. Sintering may be controlled by harboring the active catalyst nanoparticles such that surface movement is restricted by surface potential wells (nanochannels) where the particle potential energy is minimized. We accomplished this by embedding of the catalytic nanoparticles (NPs) in 2–4 nm wide shallow channels or "docking stations" oriented normal to the CNT surface resulting in superior FT-catalyst stability. The resulting structural change of the outer CNT surface caused by the formation of docking stations leads to vastly increased surface roughness which is thought to affect the ordering of atomic carbon in the CNT surface layer. The observed long-term stability of the CNT supported FT metal catalysts may result from the synergy caused by the harboring effects of docking stations, increased surface roughness and amplified reactivity of the CNTs outer layer. The confinement or harboring of the Fischer–Tropsch-catalytic particles in the docking stations along the CNT walls is described for the first time and we believe that this discovery may be quite general and apply to various other catalytic processes.

A combination of high resolution transmission and scanning transmission electron microscopy (TEM/STEM) in conjunction with electron energy loss spectroscopy (EELS) helped determine the general structure of the docking stations and assisted in identifying the presence of ultra small FT-catalyst particles within the docking stations. The work further addressed (a) what caused the formation of the docking stations on CNT surfaces, (b) what controlled the size (depth and width) and frequency of docking stations on CNT surfaces, (c) the spatial relationship of the ultra small FT catalyst particles inside the docking stations before and after FT synthesis, and (d) the role the docking stations play in protecting catalyst particles from sintering.

2 Experimental

2.1 Catalyst Preparation

Carbon nanotubes were obtained through catalytic decomposition of C_2H_2 at 700 and 800 °C over Fe-supported on $CaCO_3$ (aragonite) as described elsewhere [17, 30]. Purification of the CNTs was performed using 30–55% HNO_3 solution. Catalysts with 5 and 10% Fe supported on CNTs were prepared using incipient wetness (IW) impregnation process.

The samples were dried (120 °C overnight) and calcined (heating in nitrogen at 220 °C for 2.5 h) to decompose the salts. The catalysts were tested in a fixed bed micro reactor after reduction in H_2 at 350 °C and 2 bars for 24 h. At reaction temperature (275 °C) and pressure (8 bars), a flow of syngas (60% H_2, 30% CO, 10% Ar) was passed over the catalyst with similar flow rate (space velocity 2,142 h^{-1}).

2.2 Characterization Methods

Electron microscopy studies were performed using a JEOL 2010F STEM outfitted with a URP pole piece, GATAN 2000 GIF, GATAN DigiScan II, Fischione HAADF STEM detector, and EmiSpec EsVision software. STEM images were acquired using either the high resolution probe at 2 Å or a 1 nm analytic probe. STEM images were then deconvolved using the Lucy–Richardson algorithm [31]. EELS mapping was performed using the 1 nm probe, alpha of 20 mrad, and a beta of 6 mrad. Elemental intensity maps shown were derived from core edge intensity obtained after background subtraction using an integration window ranging from 10 to 30 eV depending on the edge.

3 Results and Discussion

Figure 1a illustrates the synthesized CNTs and Fig. 1b shows the scanning transmission electron microscope (STEM) image of surface wells or docking stations that have been formed on a multi-walled CNT exterior surface. Each docking station consists of a 2–7 nm deep nanochannel with diameter varying from 2 to 4 nm. Figure 1c is a close-up view of nine docking stations that harbor 1–2 nm-sized catalyst NPs at the bottom and sides of each nanochannel. These docking stations and their characteristic structure were imaged by enhancing the signal to noise ratio for carbon by using a small mrad detection angle in high resolution (HR) STEM mode which enhances the carbon signal at the edges of the CNT walls. The harboring capacity of catalyst NPs inside docking stations is evident both before and after FTS synthesis with little change observed as a result of FTS (confirmed using HR-TEM/STEM to study any changes in the exterior CNT's structure/morphology and location of surface wells including a comparison of the size of catalyst particles as well as size of docking stations). Figure 1d and e are high resolution TEM and STEM images of a CNT surface after FTS synthesis and illustrate location and size of catalyst particles. The TEM in Fig. 1d reveals significant surface roughness at the CNT exterior and also the presence of crystalline iron catalyst particles that are located near the

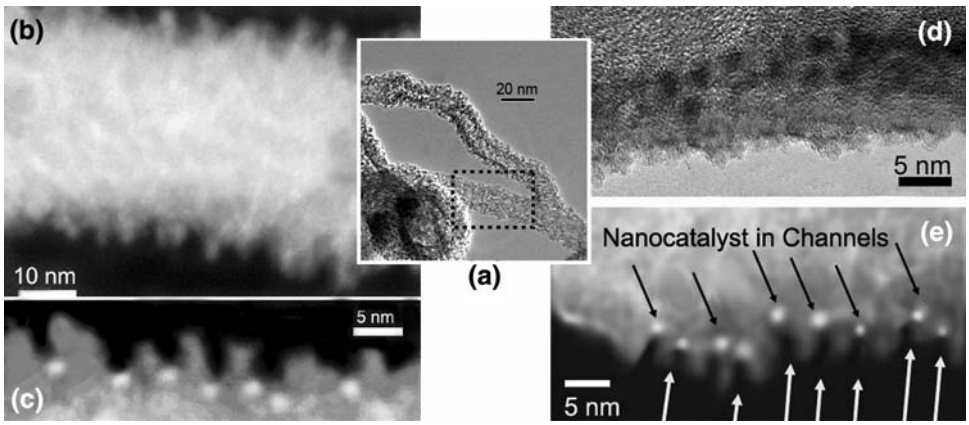

Fig. 1 **a** TEM image of synthesized CNTs; **b** HR-STEM image of carbon nanotube with nanosized docking stations along surface; **c** magnified view showing docking stations with Fe-NPs at the bottom and/or sides of the nanochannels; **d** HR-TEM illustrating high surface roughness at CNT exterior and presence of crystalline Fe-nanoparticles (*dark spots*) aligned near surface; **e** HR-STEM illustrates Fe catalyst particles at the end of some nanochannels that form normal to the CNT surface. Images **d** and **e** are taken within similar location along CNT surface

CNT surface. HR-STEM in Fig. 1e of a similar location furthermore illustrates iron catalyst particles lodged at the end of nanochannels (docking stations). The nanochannels contribute to the observed surface roughness at the CNT surface.

The excellent stability of the CNT-Fischer–Tropsch catalyst system (standard FTS conditions: 275 °C, 8 bars, H_2:CO = 0.5) and resultant carbon monoxide (CO) conversion efficiency is shown in Fig. 2. The plot of the catalytic activity in terms of conversion of CO shows no decrease in conversion efficiency with 10% Fe supported on CNT surfaces for over 120 h on stream.

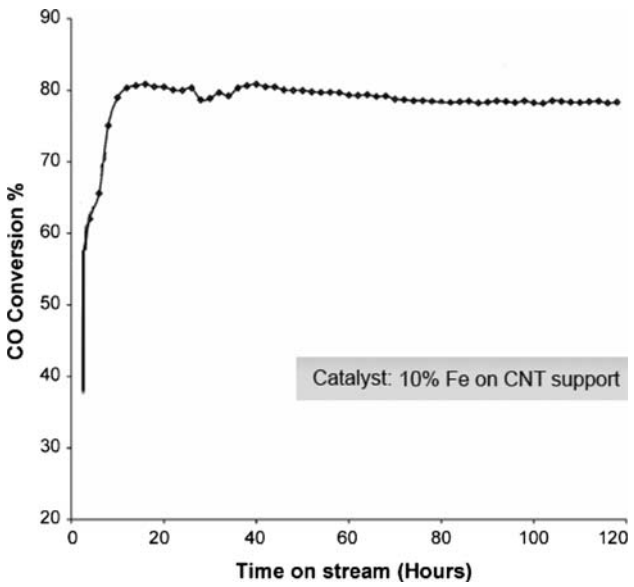

Fig. 2 CO conversion efficiency for Fisher–Tropsch synthesis using 10% Fe catalyst supported CNTs with docking stations

Additional catalyst samples that employed a urea deposition precipitation method for adding various amounts of Fe and promoters including Cu and K (0.25%) and their activities were compared to the current sample material elsewhere [17]. We determined that the presence of docking stations is a common characteristic of all the CNTs used in the preparation of the highly stable FT catalysts [17]. Against this background the existence of docking stations clearly plays a dominant role in the observed catalyst stability. The following TEM/STEM and EELS data focuses on the catalyst system that utilized 10% Fe (Fig. 2) and no promoters on CNT surfaces.

In general, metal NPs deposited on oxide or carbon tend to migrate and agglomerate on a support surface to form larger, less active particles during the catalytic process. The high degree of stability on stream during FTS with the current samples suggests that the catalyst did not deactivate or sinter appreciably. The 1–2 nm Fe particles are visibly well dispersed and harbored in the nanochannels of the docking stations along the CNT surface (Fig. 1c). Further, the effective surface area of 1–2 nm sized iron is much higher compared to unsupported or supported Fe catalysts where the particle size typically ranges from 5 to 100 nm.

The $CaCO_3$ support used for CNT synthesis consisted of micron-scale aragonite particles. The as-synthesized CNTs were washed with HNO_3 for purification and removal of any residual $CaCO_3$. Despite the acid wash calcium remained in the CNT system as shown in the dark field DF-STEM image in Fig. 3a. A dense population of uniformly distributed 1–2 nm-sized Ca as well as Fe NPs was identified using electron energy loss spectroscopy (EELS). EELS spectrum imaging was performed and the resulting composition map in Fig. 3b illustrates simultaneously the presence of Ca-NPs in green, Fe-NPs in red and oxygen in

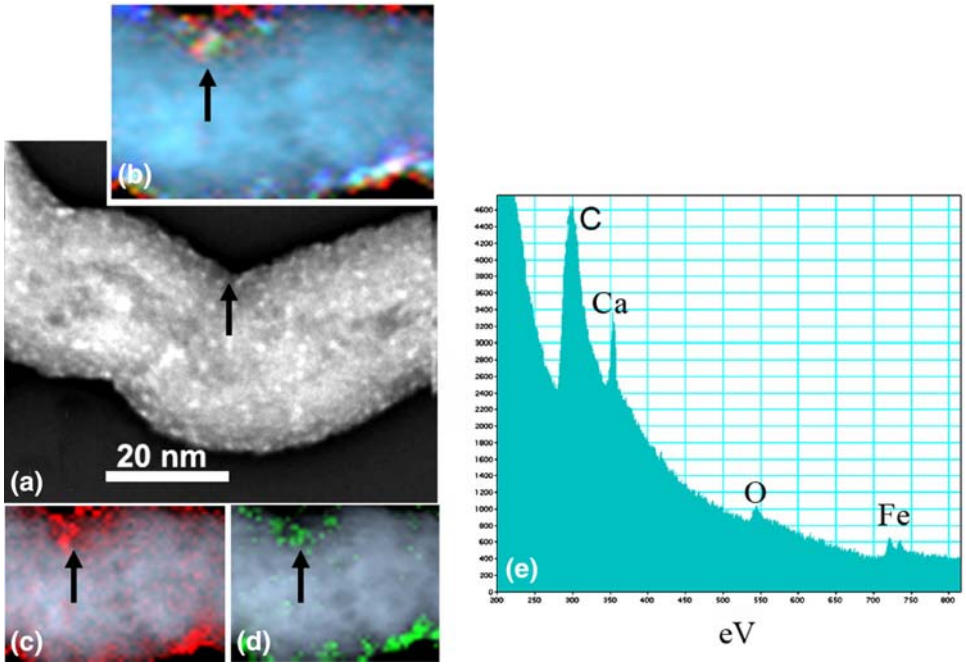

Fig. 3 *Black arrows* mark one selected area on CNT that corresponds to all images: **a** Dark field (DF)s-STEM image showing ultra-small (1–2 nm) Ca and Fe NPs dispersed on CNT surface; **b** EELS composition map simultaneously illustrates presence of Ca-NPs in *green*, Fe-NPs in *red* and oxygen in *blue*; **c**, **d** are nanoscale EELS elemental maps with analysis of Fe and Ca and their spatial distribution on CNT surface; **e** EELS spectrum taken at location of *black arrow* showing C, Ca, O, and Fe

dark blue while the carbon support is shown in light blue. The EELS spectrum image shows where the ultra small particles are anchored in the CNT surface with Ca-NPs being more abundant compared with Fe-NPs. The DF-STEM image in Fig. 3a was obtained using a detection angle of 40 mrad using a Lucy-Richardson Deconvolution method [31] using DeConvEELS software. It was determined through experimentation that this detection angle produced the best balance between the carbon and calcium dark field signals and noise level, producing the highest quality image of the Ca and Fe NPs. Here the docking station's dark field signal from the thin carbon on the CNT edges is greatly reduced by the larger detector scattering angle in order to make the Ca and Fe NPs clearly visible due to their larger atomic number, hence, larger scattering angle and, therefore, the docking stations are not visible in Fig. 3a. Spatially resolved EELS at the nanoscale is well established [32, 33] and composition mapping was performed on the CNT surface to distinguish the presence of Ca-NPs versus Fe-NPs on the carbon support (2b). Relative color intensities in the elemental display maps (Fig. 3c, d) qualitatively correlate to the absolute amounts of an element present. EELS-spectrum imaging was chosen over EDS mapping due to the superior sensitivity of EELS to light elements, particularly carbon and oxygen. This allows the use of a short dwell time of 0.1 s, which shortens mapping times considerably compared to the EDS mapping of light elements and minimizes the effects of sample instability and carbon deposition. Figure 3e is an individual EELS spectrum showing C, Ca, O, and Fe observed in a particular docking station and was taken in the location indicated by the black arrows in Fig. 3. EELS spectrum imaging in Fig. 4 clearly shows the spatial relationship between the Ca and Fe-NPs and the CNT docking stations.

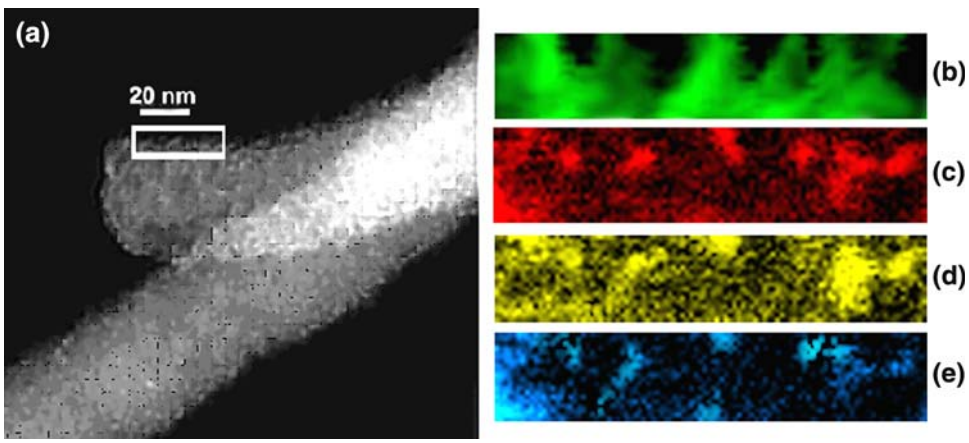

Fig. 4 **a** HR-STEM of 2 neighboring CNTs with catalyst in docking stations. Insert at CNT exterior shows area where spatially resolved EELS elemental mapping were performed; **b** carbon signal shows surface channels and contours location of docking stations; **c** relative Fe signal showing presence of Fe-NPs inside docking stations; **d** relative Ca signal showing presence of Ca-NPs lining docking stations; **e** relative oxygen signal on CNT surface

Analysis was done at the edge of a CNT (Fig. 4a) and the carbon signal corresponds to the docking stations shown in Fig. 4b while the presence of Fe and Ca inside the docking stations is shown in Fig. 4c and d, respectively. The relative oxygen signal is illustrated in Fig. 4e. The presence of ultra small (~1 nm) Fe-NPs seems to always correlate with 1–2 nm Ca-NPs that are present on the contours of the CNT docking stations. EELS elemental maps described in Fig. 4 clearly demonstrate the confinement of the ultra small Fe-FT catalyst particles within the docking stations of the CNTs along with abundant Ca-NPs. Some channels are seeded with Ca-NPs and lack Fe-NPs. While calcium is a promoter for the iron catalyst, at high concentrations it decreases the catalytic activity of the iron. It remains to be defined how the high concentration of calcium in the vicinity of the iron nanoparticle does not appear to negatively impact the catalytic activity.

The event that led to the incorporation and confinement of Ca-NPs into the CNT walls was determined to occur during the thermal treatment step of the catalyst particles rather than the CNT growth step itself as confirmed by STEM imaging and elemental analyses of CNTs during the various synthesis stages (CNT growth followed by acid washing, followed by iron precursor impregnation, followed by thermal treatment at 220 °C in nitrogen). Acid washing of the as-formed CNTs removed the bulk of aragonite support and only minor amounts remained on residual CNTs after acid wash. Ca-ions coat the acid washed CNTs prior to calcination treatment, perhaps along defect sites on CNTs surfaces. The high density of ultra-small Ca-NPs incorporated and confined in the CNT surface layers and inside docking stations as shown in Figs. 3a and 4d could only be observed after calcination treatment at 220 °C. We expect that Ca may have catalytically promoted the disruption of carbon bonds in the CNT outer walls caused by highly localized gasification along the CNT surface while the samples were treated at 220 °C under nitrogen. After the thermal treatment/gasification step, STEM shows CNTs to have a highly defined nanochannel structure where each surface channel is separated by a carbon ridge, leading to the observed alternating nanoscale "ridge and valley" morphology (Fig. 1b). In TEM mode the individual carbon ridges are distinguished as fullerenes (Fig. 5) which occur on each side of a nanochannel or docking station. Some ridges are constructed of two or more vertically aligned fullerenes, which produces deeper channels (Fig. 5b). A model of the steps that lead to fullerene formation and docking stations is illustrated in Fig. 6. We observe a cause and effect: fullerenes and nanochannels form after the calcination step on CNTs that had a residual Ca thin film on their surfaces after acid wash. A buckling effect is also observed for the outer layers of most CNTs while inner walls are fairly straight. Ca tunnels into outer CNT walls during calcination step. On an atomic scale, disruption of the outer walls by Ca results in the bending or rolling up of graphite planes which leads to abundant fullerene formation as shown in the TEM images in Fig. 5a, b. This also increases the local anisotropy of the CNT exterior surface which results in an increase in active sites. If calcium penetrates into lower laying walls we observe stacked-up fullerene structures and an increase in the depth of the docking stations (Fig. 6). Since CNTs in general represent an intermediate state between sp^2- and sp^3-hybridization [15], any disruption of short or long-range carbon bonds in the CNT surface will affect the electronic structure for those particular surface carbon atoms and with it the nanostructure of the carbon material which essentially determines CNT's performance as a catalyst support. Buckling of the outer walls caused by Ca may have a "stress" effect comparable to that observed for carbon materials subjected to intense axial compression or other mechanical deformation, all of which will ultimately alter the short- and long-range ordering of atomic carbon and with it the macroscopic properties. This results

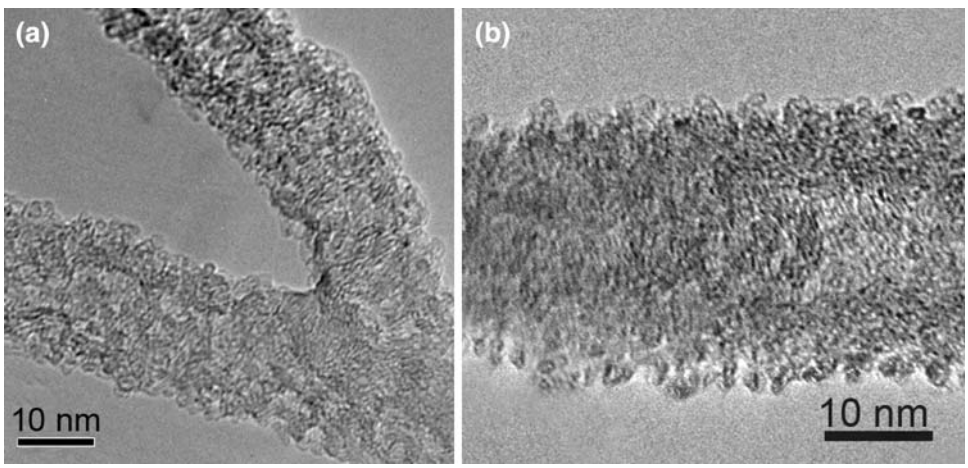

Fig. 5 **a**, **b** HRTEM of CNT with abundant fullerenes on surface lining nanochannels. Fullerenes are connected to buckled CNT outer walls

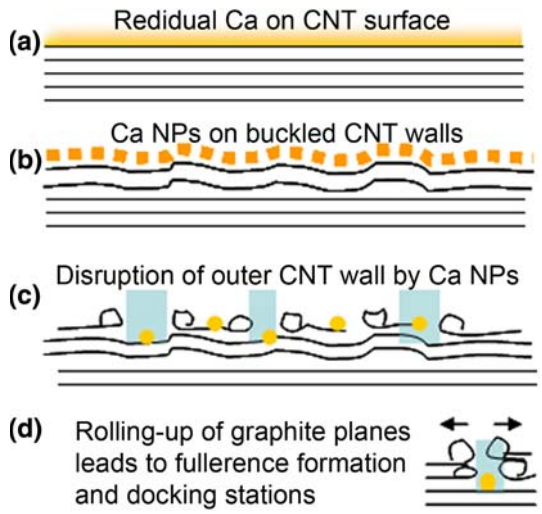

Fig. 6 Schematic model of fullerene formation and presence of docking stations on CNT exterior. Calcium is shown in *orange* and docking stations are represented in *blue*; *lines* represent CNT and *circles* represent fullerenes. **a** Residual calcium deposited after acid washing of CNTs (CNT formation used iron catalysts on aragonite support) leads to calcium thin film formation on carbon nanotube exterior; **b** buckling of outer CNT walls and formation of Ca nanoparticles (NPs) occurs during calcinations step; **c** Ca tunnels deeper into outer CNT walls during calcinations step; disruption of outer walls by Ca leads to selective rolling up of graphite planes and fullerene formation and starts the formation of a shallow docking station; **d** when Ca disrupts several CNT outer walls (tunnels deeper), deeper docking stations are formed and we observe multiple fullerenes typically stacked up on top of each other on each side of the docking station. Ca NPs are often found at the bottom or sides of the docking stations

in the synthesis of a highly advanced metal and/or metal oxide/carbide catalyst system supported on carbon nanostructures (catalyst is harbored inside docking stations). The Fe-NPs are protected from migration and coalescence on the active carbon surface (outer CNT wall) and the effective surface area for FTS is maximized. The 3D morphology of the outer CNT walls plays a major role such that Fe-NPs are harbored in potential docking stations or surface wells where energy is minimized and restricts the catalyst particles from migrating out of these areas. The surrounding fullerene-ridges provide an activation energy barrier to Fe-NPs migration. The ultra-small particle size and high surface area of these Fe catalysts translates to a high turnover frequency and higher catalytic activity for FTS.

4 Conclusions

The docking stations on the CNT surfaces provide long-term stability, combined with high yields of the Fe/CNT catalysts which would lead to cost advantage for synthetic fuels derived from FTS. Residual calcium from the CNT synthesis process is shown to play a significant role in the formation of the docking stations. The localized oxygen found along the outline of the docking stations may be important for oxidation catalysis with oxygen localized on defect sites on the carbon structures. On the other hand the presence of highly dense populated ultra-small Ca-NPs on the surface of CNTs may provide novel scaffolds for other research areas, one such area may be synthetic bone growth. We believe these docking stations can harbor variety of metal catalyst particles for industrially important applications.

References

1. Grow RJ (2006) Carbon nanotubes 187
2. Guldi DM (2007) Nature 447(7140):50
3. Serp P, Corrias M, Kalck P (2003) Appl Catal A Gen 253(2):337
4. Balasubramanian K, Burghard M (2005) Small 1(2):180
5. Zhang J, Liu X, Blume R, Zhang A, Schloegl R, Su DS (2008) Science 322(5898):73
6. Goldsmith BR, Coroneus JG, Khalap VR, Kane AA, Weiss GA, Collins PG (2007) Science 315(5808):77
7. Song X, Liu S, Yan H, Gan Z (2008) Electronic components and technology conference ECTC 2008 (58):2091
8. Niu JJ, Wang JN, Jiang Y, Su LF, Ma J (2007) Microporous Mesoporous Mater 100(1–3):1
9. LaBrosse MR, Shi W, Johnson JK (2008) Langmuir 24(17):9430
10. Mendoza E, Rodriguez J, Li Y, Zhu YQ, Poa CHP, Henley SJ, Romano-Rodriguez A, Morante JR, Silva SRP (2007) Carbon 45(1):83
11. Bahome MC, Jewell LL, Hildebrandt D, Glasser D, Coville NJ (2005) Appl Catal A Gen 287(1):60
12. Bezemer GL, Falke U, van Dillen AJ, de Jong KP (2005) Chem Commun (6):731
13. Bezemer GL, Bitter JH, Kuipers HPCE, Oosterbeek H, Holewijn JE, Hohannes E, Xu X, Kapteijn F, van Dillen A, de Jong KP (2006) J Am Chem Soc 128:3956
14. Pham-Huu C, Ledoux MJ (2006) Top Catal 40(1–4):49
15. Zhang J, Su D, Zhang A, Wang D, Schloegl R, Hebert C (2007) Angew Chem Int Edit 46(38):7319
16. Davis BH (2007) Ind Eng Chem Res 46(26):8938
17. Bahome MC, Jewell LL, Padayachy K, Hildebrandt D, Glasser D, Datye AK, Coville NJ (2007) Appl Catal A Gen 328(2):243
18. Bezemer GL, Radstake PB, Falke U, Oosterbeek H, Kuipers HPCE, van Dillen AJ, de Jong KP (2006) J Catal 237(1):152
19. Dry ME, Hoogendoorn JC (1981) Catal Rev—Sci Eng 23(2):265
20. Storch HH, Golumbic N, Anderson RB (1951) The Fischer–Tropsch and related syntheses. Wiley, New York
21. Boerrigter H, den Uil H, Calis H-P (2003) Proceedings of an expert meeting, Strasbourg, September 30–October 1 2002, p 371
22. Chum HL, Overend RP (2001) Fuel Process Technol 71(1–3):187
23. Tijmensen MJA, Faaij APC, Hamelinck CN, van Hardeveld MRM (2002) Biomass Bioenergy 23(2):129
24. O'Brien RJ, Xu L, Bao S, Raje A, Davis BH (2000) Appl Catal A Gen 196(2):173
25. Bezemer GL, Bitter JH, Kuipers HPCE, Oosterbeek H, Holewijn JE, Xu X, Kapteijn F, van Dillen AJ, de Jong KP (2006) J Am Chem Soc 128(12):3956
26. Chen W, Fan Z, Pan X, Bao X (2008) J Am Chem Soc 130(29):9414

27. Jackson SD (2006) Chem Eng J (Amsterdam, Netherlands) 120(1–2):119
28. Forzatti P, Lietti L (1999) Catal Today 52(2–3):165
29. Pan X, Fan Z, Chen W, Ding Y, Luo H, Bao X (2007) Nat Mat 6(7):507
30. Magrez A, Seo JW, Kuznetsov VL, Forro L (2007) Angew Chem Int Edit 46(3):441
31. Ishizuka K, Kimoto K, Bando Y (2003) Microsc Microanal 9(suppl 2):832
32. Egerton RF (1999) Electron Microsc 48(6):711
33. Muller DA, Tzou Y, Raj R, Silcox J (1993) Nature 366(6457):725